J Mol Model (2011) 17:2797–2804
DOI 10.1007/s00894-011-0961-3

ORIGINAL PAPER

Theoretical study of isotope effects on the stereodynamics of H^++HD and its isotopic variant D^++HD

Junsheng Chen · Luoqiu Wang

Received: 5 September 2010 / Accepted: 5 January 2011 / Published online: 2 February 2011

Abstract The stereodynamics for H^++HD and its isotopic variant D^++HD were studied with a quasi-classical trajectory (QCT) method at a collision energy of 0.7 eV on the ground $1^1A'$ potential energy surface (PES). The polarization-dependent differential cross-sections (PDDCSs) in the center-of-mass frame are presented here. Furthermore, the distribution of the angle between **k** and **j′**, $p(\theta_r)$ and the distribution of the dihedral angle $p(\phi_r)$ were calculated and are discussed. The results indicate that isotopic substitution exerts substantial effects on the differential cross-section and the product's rotational polarization.

Keywords Stereodynamics · Quasiclassical trajectory theory (QCT) method · Isotope effect

Introduction

In interstellar chemistry, it is well known that a series of reactions are induced by the H_3^+ ion, and that this subsequently leads to the formation of a great number of larger molecules [1, 2]. In addition, the H_3^+ ion is the main component of hydrogen plasmas [1]. Since it is the typical ion–molecule reaction, the H_3^+ system has always been used to test the quality of a new theory or experiment [2]. Due to its fundamental importance, the H^++H_2 reaction and its isotopic variants have been investigated widely. Over the last decade, many theoretical and experimental studies have been carried out on this system [1–24]. In 2000 and 2006, two meetings entitled "Physics, Chemistry and Astronomy of H_3^+" were held by the Royal Society (see papers from discussion meetings on the subject: [22, 23]). In these meetings, H_3^+ was discussed from a variety of perspectives. On the other hand, previous studies on the Rydberg atom reaction H(n)+D_2→HD+D(n) using the Rydberg H-atom translation spectroscopy technique [13, 14] have shown quite similar results to those of the ion–molecule reaction H^++D_2→HD+D^+ as calculated by the quasiclassical trajectory (QCT) method [21]. Thus, we can also use the ion plus diatom exchange process to investigate Rydberg atom plus diatom reaction dynamics. In order to fully understand the dynamics of an elementary reaction, it is necessary to study both the scalar and the vector properties of the reaction. In relation to chemical stereodynamics, Hsu et al. employed a new buffer field design in experimental measurements to deal with the orientation of the rotational angular momentum of a product molecule [25]. Aoiz et al. developed a complete classical treatment of the **k-j′-k′** vector correlation for atom–diatom reactions [26], which was applied in order to study the Li+HF(v=1, j=1, m=0) reaction and other triatomic systems, and yielded results that were in good agreement with the experimental ones. Miranda and coworkers [24, 27] employed a quantum treatment to describe the stereodynamics of the H+D_2 reaction. They analyzed their calculated state-to-state results and found that the agreement between the quantum and quasiclassical calculations was quantitative for the polarization parameters. Based on density matrix techniques, angular momentum algebra, and their knowledge of the scattering matrix, they also presented a theoretical quantum method for describing the stereodynamics of four-atom reactions of the type AB+CD ↔ ABC+D, and applied their method to H_2+OH↔ H_2O+H to reveal vector properties such as

J. Chen · L. Wang (✉)
College of Physics Science and Technology,
China University of Petroleum Dongying,
Shandong 257061, People's Republic of China
e-mail: wlq_911226@163.com

the state-specific correlations between the polarizations of the diatomic molecules, their incident and recoil directions, etc. [28].

H^++H_2 and its isotopic variants are governed by an insertion mechanism, and have been investigated by different methods. This reaction family usually has three product channels: reactive charge transfer (RCT), nonreactive charge transfer (NRCT) and reactive noncharge transfer (RNCT). Han and coworkers studied the D^++H_2 and H^++D_2 reactions, focusing on the nonadiabatic competition of these channels [15]. Their theoretical results agree with the experimental results quite well. Very recently, Han and coworkers also demonstrated that the three product channels present different energy-dependent isotope effects, with the most pronounced being predicted for the RNCT channel [16]. In addition, a great deal of study has focused on using statistical quantum, time-independent quantum mechanical, approximate quantum wavepacket, and quasi-calassical trajectory approaches to investigate the H^++H_2, D^++H_2 and H^++D_2 reactions [17–19]. For example, Jambrina et al. carried out WP-EQM (wavepacket exact QM), QCT and statistical quasi-classical trajectory (SQCT) calculations, and investigated the H^++D_2 reaction for a range of collision energies, starting from the reaction threshold to 1.3 eV [2]. Song et al. studied the H^++H_2 reaction with the QCT method and found that it is a complex-formation reaction [20]. All of these results indicate that the RNCT process is governed by an insertion mechanism.

Many theoretical studies of the H_3^+ system have been carried out, but our understanding of this system is still incomplete. In order to gain more information about the isotope effect on this system, we carried out QCT calculations for the following reactions:

H^++HD (v=0, j=0) → H_2+D^+ (channel 1) → HD+H^+ (channel 2)
D^++HD (v=0, j=0) → DH+D^+ (channel 1) → D_2+H^+ (channel 2)

at a low collision energy of 0.7 eV, and we neglected all nonadiabatic processes.

Computational methods

Vector correlation and distribution

In Fig. 1, the center-of-mass (CM) frame is chosen to describe the correlations among **k**, **k′**, and **j′**. The x-z plane is the so-called scattering plane containing the relative velocity vector **k** of the reagent and the relative velocity **k′** of the product. The initial relative velocity vector **k** is along the z axis. **j′** is the rotational momentum of the product. θ_t is the angle between the relative velocity of the product and the relative velocity of the reagent, and is called the scattering angle. The angle θ_r is the so-called polar angle between the z axis and the final rotational angular momentum. The azimuth angle φ_t and θ_r, together determine the direction of the final rotational angular momentum **j′**.

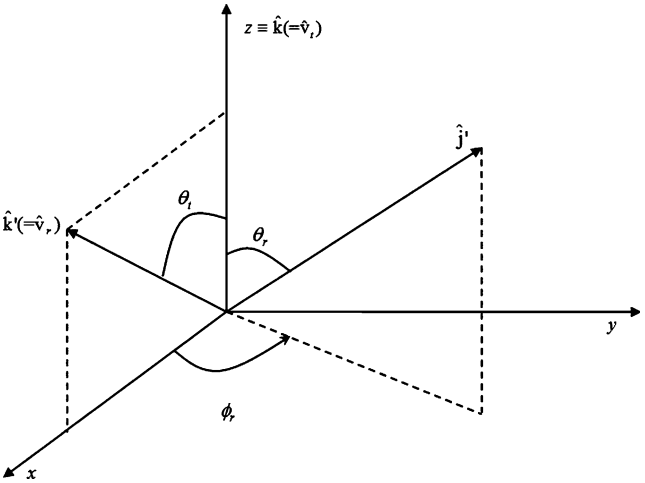

Fig. 1 The center-of-mass frame used to describe the correlations among **k**, **k′**, and **j′**

In the CM frame, the full three-dimensional angular distribution associated with **k**, **k′**, and **j′** is represented by a set of generalized polarization-dependent differential cross-sections (PDDCSs) [29–32]. The fully correlated CM angular distribution is written as the sum [33]

$$p(\omega_t, \omega_r) = \sum_{kq} \frac{[k]}{4\pi} \frac{1}{\sigma} \frac{d\sigma_{kq}}{d\omega_t} C_{kq}(\theta_r, \phi_r), \quad (1)$$

where ω_t=θ_t,ϕ_t and ω_r=θ_r,ϕ_r refer to the coordinates of the unit vectors **k′** and **j′** along the directions of the product's relative velocity and angular momentum vectors in the CM frame, respectively [34]. $[k]$=$2k$+1, $(1/\sigma)(d\sigma_{kq}/d\omega_t)$ is a generalized polarization-dependent differential cross-section (PDDCS), and $C_{kq}(\omega_r)$ are modified spherical harmonics. In our work, $\frac{2\pi}{\sigma}\frac{d\sigma_{00}}{d\omega}$, $\frac{2\pi}{\sigma}\frac{d\sigma_{20}}{d\omega}$, $\frac{2\pi}{\sigma}\frac{d\sigma_{22+}}{d\omega}$ and $\frac{2\pi}{\sigma} \times \frac{d\sigma_{21-}}{d\omega}$ are calculated. PDDCSs are expanded up to $\mathbf{k}_1$=7, and they show good convergence.

Customarily, double-vector correlations (**k**-**j′**, **k**-**k′** or **k′**-**j′**) can be expanded as a Legendre series. Thus, **k**-**j′** is expanded as the distribution function $p(\theta_r)$ [33, 35–37]:

$$p(\theta_r) = \frac{1}{2} \sum_k [k] a_0^k p_k(\cos\theta_r). \quad (2)$$

The a_0^k coefficients are polarization parameters:

$$a_0^k = \langle p_k(\cos\theta_r) \rangle. \quad (3)$$

The angular brackets indicate an average over all reaction trajectories. When $p(\theta_r)$ is expanded up to k=18, it shows

good convergence. Triplet vector correlations (**k-k′-j′**) can be described by the dihedral angle ϕ_r distribution. This distribution of ϕ_r is expanded as a Fourier series [33, 35–37]:

$$p(\phi_r) = \frac{1}{2\pi}\left(1 + \sum_{n,even\geq 2} a_n \cos n\phi_r + \sum_{n,odd\geq 1} b_n \sin n\phi_r\right), \quad (4)$$

where $a_n = 2\langle \cos n\phi_r \rangle$ and $b_n = 2\langle \sin n\phi_r \rangle$. In this paper, $p(\phi_r)$ is expanded to n=24, and it shows good convergence. The direction of **j′** can be defined by the angle θ_r and ϕ_r. In the CM frame, the distribution $p(\theta_r,\phi_r)$ can be expanded as

$$p(\theta_r,\phi_r) = \frac{1}{4\pi}\sum_{kq}[k]a_q^k C_{kq}(\theta_r,\phi_r)^*$$

$$= \frac{1}{4\pi}\sum_{k}\sum_{q\geq 0}\left[a_{q\pm}^k \cos q\phi_r - a_{q\mp}^k i \sin q\phi_r\right] C_{kq}(\theta_r,0). \quad (5)$$

During the calculation, the parameter a_q^k is evaluated via

$$a_{q\pm}^k = 2\left\langle C_{k|q|}(\theta_r,0)\cos q\phi_r \right\rangle_{\text{k even}} \quad (6)$$

$$a_{q\pm}^k = 2i\left\langle C_{k|q|}(\theta_r,0)\sin q\phi_r \right\rangle_{\text{k odd.}} \quad (7)$$

In this work, $p(\theta_r,\phi_r)$ is expanded up to k=7, which converged sufficiently.

Quasi-classical trajectory calculations

In our QCT calculations, the KBNN potential-energy surface (PES) was employed. Kamisaka et al. modified the diatomics-in-molecules potential energy surface (DIM PES) and denoted the modified PES "KBNN PES" [8]. This consists of a 3×3 DIM potential matrix and three-body correction terms. Compared with the DIM PES, the KBNN PES has two distinguishing characteristics: first, the KBNN PES has a slightly shallower well in the lower PES; second, the long-range attractive force in the lower PES is smaller in KBNN. By diagonalizing the 3×3 KBNN potential matrix, the three adiabatic surfaces (the ground $1^1A'$ surface, the first excited $2^1A'$ surface, and the second excited $3^1A'$ surface) can be obtained. The $3^1A'$ surface is quite high, and the energy of the cross region between the $1^1A'$ and $2^1A'$ surfaces is about 2.2 eV with respect to the asymptotic energy of the reagents. In our study, the collision energy selected was 0.7 eV, which is far below the cross region between the $1^1A'$ and $2^1A'$ surfaces. At such a low collision energy, nonadiabatic transitions [38, 39] will not take place. Thus, it is reasonable to perform the present calculation on the ground surface ($1^1A'$) with a potential well of ~4.5 eV. Besides, the QCT method we used in this work is the same as that used by Han et al., who first applied the QCT method to calculate product rotational alignment in 1993 [40], which made it feasible to directly compare theoretical calculations with experimental measurements of product polarizations.

Results and discussion

Figure 2 shows the total reaction probability $P_R(E_{collision})$as a function of the collision energy $E_{collision}$ for the H^++D_2 (v=0, j=0) →D^++HD reaction with the total angular momentum J=0. In the figure, the QCT results are compared with the weavepacket exact quantum mechanical (WP-EQM) ones (the black line) [2]. Despite the oscillations in the QM results over the investigated energy range, the QCT-calculated reaction probability agrees reasonably well with the WP-EQM result. Of course, there are some differences between the QCT and WP- EQM results, as indicated in [2]. However, based on the reasonable agreement shown above, we believe that such differences will not significantly influence the general trend in the stereodynamical properties obtained from the present QCT calculations.

The QCT PDDCSs of the H_2, HD and D_2 product molecules from the two reactions with two different channels are presented in Fig. 3. The PDDCS [$(2\pi/\sigma)(d\sigma_{00}/d\omega_t)$] describes the correlation of the **k-k′** or the scattering direction of the product. As can be seen in Fig.3a, for all product channels, $(2\pi/\sigma)(d\sigma_{00}/d\omega_t)$ is roughly symmetric with respect to 90°, which demonstrates that a complex with a long lifetime (compared to the mean rotational period) forms during these reactions [2, 14, 20]. Although the values of $(2\pi/\sigma)(d\sigma_{00}/d\omega_t)$ are quite small,

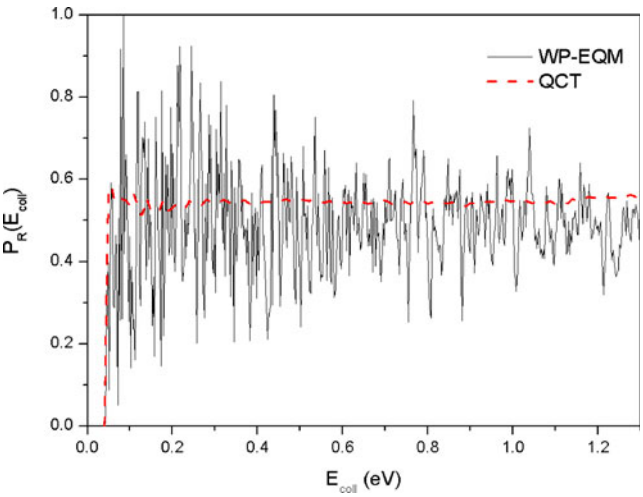

Fig. 2 Comparison of QCT and WP-EQM total reaction probabilities $P^{J=0+}(E_{collision})$ as a function of the collision energy $E_{collision}$ with J=0, for the H^++D_2 (v=0, j=0) → D^++HD reaction. *Red dashed line* QCT results. *Black solid line* WP-EQM results

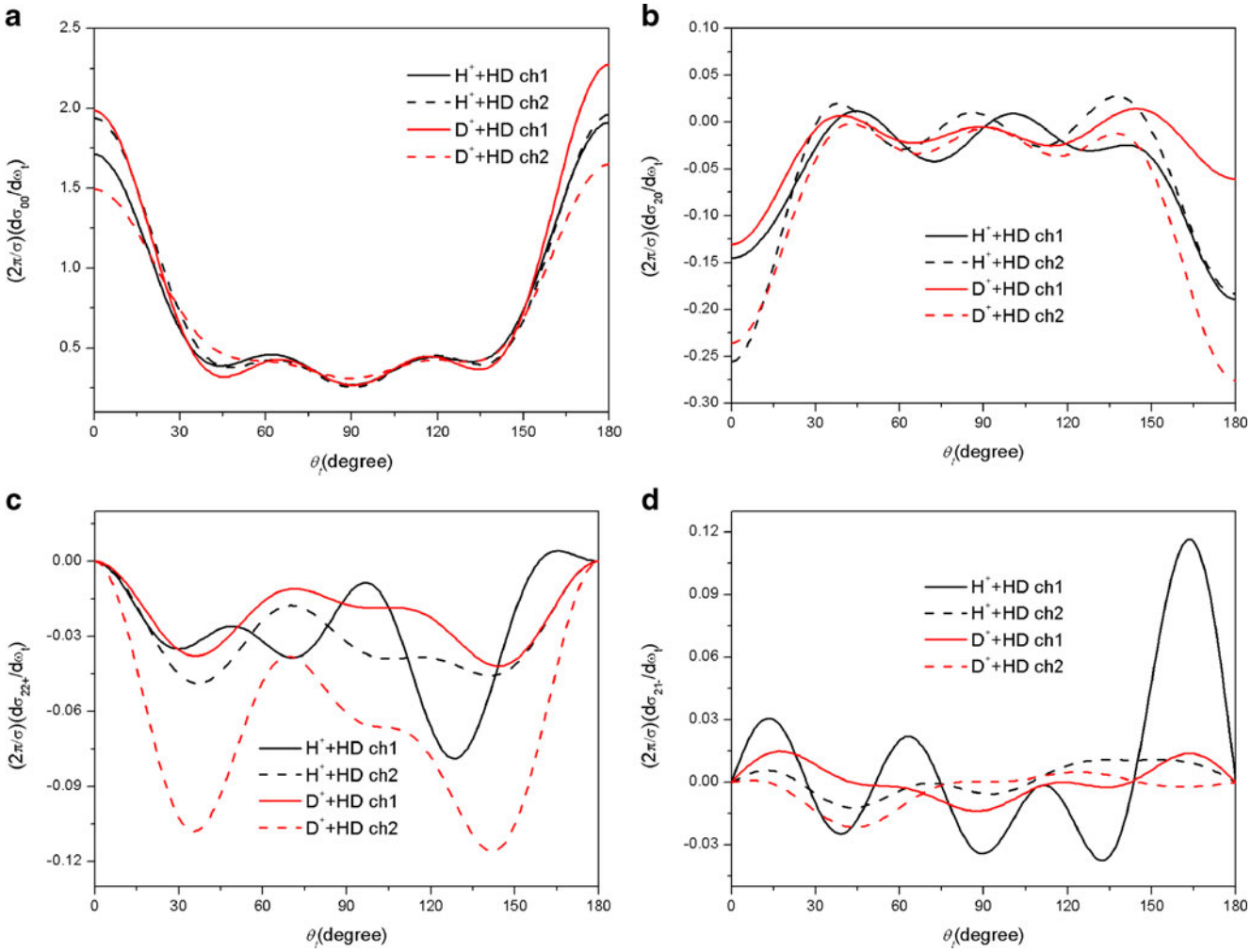

Fig. 3a–d Four PDDCSs of the products at a collision energy of 0.7 eV. **a**–**d** show the PDDCSs with (k, $q\pm$)= (0,0), (2,0), (2,2+), (2,1−), respectively. The reactions H^++HD → H_2+D^+, H^++HD →HD + H^+, D^++HD →HD+D^+, and D^++HD → D_2 + H^+ are depicted by a *black solid line*, a *black dashed line*, a *red solid line* and a *red dashed line*, respectively

there are still some differences among these reactions. For the H^++HD reaction, the products of channel 1 show a slight backward bias, while the $(2\pi/\sigma)(d\sigma_{00}/d\omega_t)$ values of the products of channel 2 are obviously symmetric with respect to 90°. For the D^++HD reaction, the products of channel 1 still slightly favor backward scattering, while the forward scattering of products is relatively strong in channel 2. In addition, in each reaction with different product channels, the distribution of the scattered products shows an increased tendency for backward scattering with an increasing mass factor $\cos^2\beta$ [defined by $\cos^2\beta = m_L m_{L''}/(m_L + m_{L'})(m_{L'} + m_{L''})$ for the L+L′L″ →LL′+L″ reaction]. In Table 1, we show the mass factors we calculated for these reactions. The distribution of $(2\pi/\sigma)(d\sigma_{20}/d\omega_t)$, which is related to $\langle P_2(\cos\theta_r)\rangle$, is shown in Fig. 3b. Compared with the PDDCS $(2\pi/\sigma)(d\sigma_{00}/d\omega_t)$ values, the values of $(2\pi/\sigma)(d\sigma_{20}/d\omega_t)$ are small for all angles between 0° and 180°. It is very interesting to note that the distribution of $(2\pi/\sigma)(d\sigma_{20}/d\omega_t)$ shows the opposite trend to that of the $(2\pi/\sigma)(d\sigma_{00}/d\omega_t)$, which implies that the product's rotational angular momentum **j′** is preferentially polarized along the direction perpendicular to **k** for these reactions. Comparing channel 1 with channel 2, we can see that the values of $(2\pi/\sigma)(d\sigma_{20}/d\omega_t)$ approach −0.5 in channel 2 of the two reactions. Therefore, we can say that, of these two channels, the products of channel 2 show

Table 1 Alignment parameters $\langle P_2(\mathbf{j}'\cdot\mathbf{k})\rangle$ calculated for H^++HD and its isotopic reaction

Reaction system	$\langle P_2(\mathbf{j}'\cdot\mathbf{k})\rangle$	Mass factor $\cos^2\beta$
H^++HD →H_2+D^+	−0.04955	0.333
H^++HD→HD+H^+	−0.0302	0.111
D^++HD →HD+D^+	−0.02669	0.444
D^++HD →D_2+H^+	−0.07039	0.166

relatively strong alignment. The PDDCSs$(2\pi/\sigma)(d\sigma_{22+}/d\omega_t)$ and $(2\pi/\sigma)(d\sigma_{21-}/d\omega_t)$, which correlate with $\langle \sin^2\theta_r \cos^2\phi_r \rangle$ and $\langle \cos\theta_r \sin\theta_r \sin\phi_r \rangle$, are displayed in Fig. 3c and d, respectively. Compared with $(2\pi/\sigma)(d\sigma_{00}/d\omega_t)$, the values of $(2\pi/\sigma)(d\sigma_{22+}/d\omega_t)$ and $(2\pi/\sigma)(d\sigma_{21-}/d\omega_t)$ are relatively small and are quite close to zero. This means that, on the whole, the product polarizations depicted by these two PDDCSs are very weak. Even so, Fig. 3c shows that the product D_2 displays relatively strong polarization at about 37° and 142° in channel 2 of the D^++HD reaction, while the polarization of the H_2 product is relatively strong at 130° in channel 1. In Fig. 3d, the distribution of $(2\pi/\sigma)(d\sigma_{21-}/d\omega_t)$ shows some oscillations in channel 1 of the H^++HD reaction. For the other reactions, the distribution of $(2\pi/\sigma)(d\sigma_{21-}/d\omega_t)$ has only very small oscillations. Thus, the distribution of the product rotational angular momentum **j′** tends to be anisotropic in channel 1 of the H^++HD reaction and in channel 2 of the D^++HD reaction.

Figures 4 and 5 show the distributions of $p(\theta_r)$ and $p(\phi_r)$ for these reactions with different product channels. As can be seen, the values of $p(\theta_r)$ and $p(\phi_r)$ are rather small, indicating that the polarization of the product is weak, which is caused by the long-lived complex formed in these reactions [14, 20]. In Fig. 4, the maximum for $p(\theta_r)$ is located at 90°, and the distribution is symmetric with respect to 90° for these reactions. Figure 5 shows the distribution of $p(\phi_r)$, which describes the **k-k′-j′** correlation. Obviously, the values of $p(\phi_r)$ are small, suggesting that the rotational alignment of the product is not strong. However, the observation that $P(\phi_r)$ is asymmetric about ϕ_r=180°, indicates the existence of product orientation. The reason for this is probably the repulsive energy between the H and D atoms. In [41–43], an impulse model for the A+BC→AB+C reaction was used to calculate the rotational alignment of the product molecules. Starting from this model [43], we have

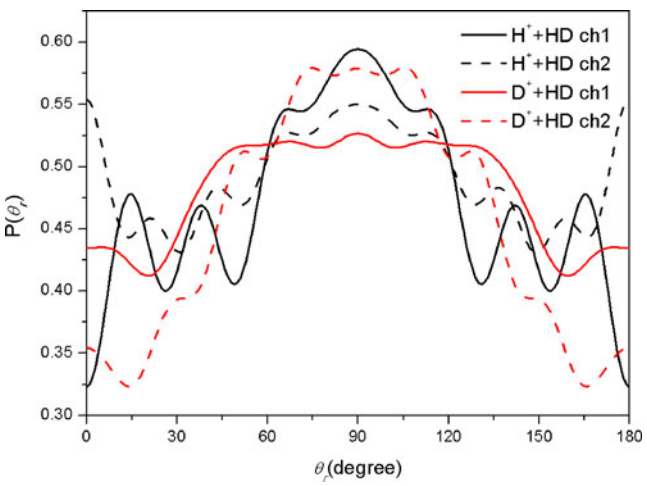

Fig. 4 The distributions of $p(\theta_r)$ for the product molecules at a collision energy of 0.7 eV. $p(\theta_r)$ describes the correlation **k-j′** for these reactions

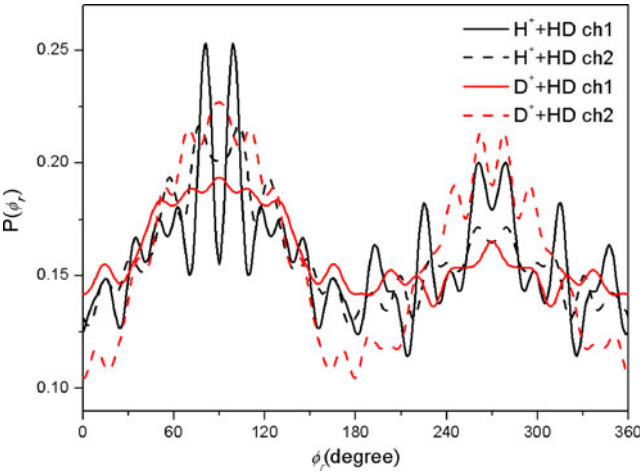

Fig. 5 The distributions of $p(\varphi_r)$ for the product molecules at a collision energy of 0.7 eV. $p(\varphi_r)$ shows the correlation **k-k′-j′** for these reactions

$$\mathbf{j}' = \mathbf{L}\sin^2\beta + \mathbf{J}\cos^2\beta + \mathbf{J_1}m_B/m_B, \quad (8)$$

where **L** is the orbital angular momentum of the reagent, **J** is the rotational angular momentum of the reagent, and $\mathbf{J_1} = \sqrt{\mu_{BC}R}(\mathbf{r}_{AB} \times \mathbf{r}_{BC})$; μ_{BC} is the reduced mass of the BC molecule, $\mathbf{r}_{AB}$ and $\mathbf{r}_{BC}$ are unit vectors where B points to A and where B points to C, respectively, and R is the repulsive energy. As we can see, in the above equation, $\mathbf{L}\sin^2\beta + \mathbf{J}\cos^2\beta$ is symmetric in these reactions, while the term $\mathbf{J_1}m_B/m_{AB}$ associated with the repulsive energy $\mathbf{J_1}$ shows a preferred direction. As a result of this preference, the products in our investigated reactions prefer right-handed rotation in the planes parallel to the scattering plane.

A comparison of the distributions of $p(\theta_r)$ for these reactions (see Fig. 4) also highlights some differences. For the H^++HD reaction, the distribution of $p(\theta_r)$ in channel 2 is broader than that in channel 1, with a lower peak position at θ_r = 90° and the other two obvious and extra peaks at 0° and 180°. Although both product channels exhibit a similar weak tendency for **j′** to be aligned along the direction perpendicular to the reagent's relative velocity **k**, it is obvious that the product's rotational alignment is stronger in channel 1. For the D^++HD reaction, the distribution of $P(\theta_r)$ in channel 1 is broader than that in channel 2, which demonstrates that in channel 1 the alignment of **j′** is weaker than that in channel 2. This polarization behavior in D^++HD is quite different from that in the H^++HD reaction. When comparing the distribution of $P(\theta_r)$ in channel 1 of the H^++HD reaction with its corresponding part in the isotopic reaction D^++HD, the oscillations in $P(\theta_r)$ are found to be less prominent in the D^++HD reaction, which shows that **j′** is almost isotropic along the **k** direction in this

reaction system. Moreover, we calculated the alignment parameter $\langle P_2(\mathbf{j}' \cdot \mathbf{k})\rangle$, which can also reflect the degree of rotational polarization of the product. The values of $\langle P_2(\mathbf{j}' \cdot \mathbf{k})\rangle$ for these reactions are shown in Table 1, and are in good agreement with the distribution of $P(\theta_r)$.

For the H+H′L (H, heavy; L, light) reaction, Han et al. [43, 44] found that the mass factor $\cos^2\beta$ [defined as $\cos^2\beta = m_L m_{L''} / (m_L + m_{L'})(m_{L'} + m_{L''})$] for the reactions L+L′L″→LL′+L″) can affect the distribution of the product's angular momentum vector. For the above reactions, the mass factor $\cos^2\beta$ also has a significant impact on the product's rotational alignment. For the D^++HD reaction, the mass factor of channel 1 (D^++HD →HD+D^+) is larger than that of channel 2 (see Table 1). As a result, the calculated values for channel 1 become less negative and the distribution of **j′** tends to become less anisotropic, while in channel 2 the rotation of the product is relatively strong aligned, as clearly shown in Figs. 3, 4, 5 and 6. A comparison of channel 1 for the H^++HD and D^++HD reactions shows the same phenomenon, which can be probably explained as follows. The total angular momentum is conserved during these reactions; that is, **j**+**L**=**j′**+**L′** (here **L** and **L′** are the reagent's and product's orbital angular momenta) [44]. Also, we have $\mathbf{j}' = \mathbf{L}\sin^2\beta + \mathbf{J}\cos^2\beta + \mathbf{J_1} m_B / m_{AB}$ [41]; under the condition that more angular momentum will be taken away by a heavier product ion, it is very likely that decreasing the mass factor will increase the anisotropy of the distribution of **j′**. In contrast, decreasing the mass factor will decrease the anisotropy of the distribution of **j′** for the H^++HD reaction, and the same rule can be applied to channel 2 of both the H^++HD→HD+H^+ and the D^++HD →D_2+H^+ reactions. Aside from this, the lifetimes of the complexes and the threshold energies differ between the reactions, which is also responsible for the differences in behavior between these reactions.

From Fig. 5, the peaks for $p(\phi_r)$ appear at 90° and 270°, which indicates that **j′** is mainly aligned along the *y* axis of the CM frame. For all reactions, the strong peak appears at φ_r ~90°, which demonstrates that the product molecules tend to show counterclockwise rotation. Upon comparing the two product channels in the H^++HD reaction, the peak is stronger in channel 1 than channel 2, which indicates that the product's rotational angular momentum in channel 1 is relatively closely oriented to the positive direction of the *y* axis. It is also clear that the distribution of $P(\phi_r)$ in channel 2 is broader than that in channel 1. For the D^++HD reaction, the peak in channel 1 is weaker than that in channel 2, which indicates that the product's rotational angular momentum is relatively closely oriented to the

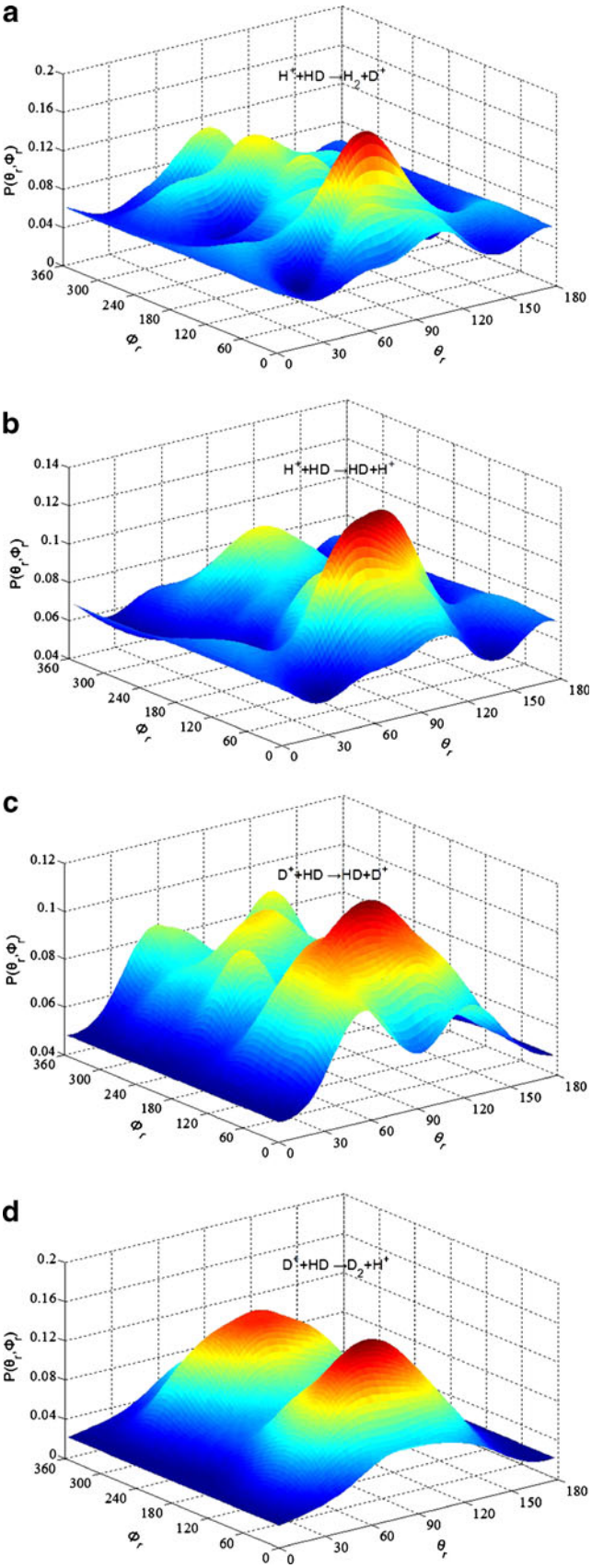

Fig. 6a–d Polar plots of $p(\theta_r, \varphi_r)$ distributions averaged over all scattering angles. **a** H^++HD →H_2 + D^+ reaction; **b** H^++HD → HD+H^+ reaction; **c** D^++HD → HD + D^+ reaction; **d** D^++HD → D_2 + H^+ reaction

positive direction of the y axis in channel 2. Upon comparing the same channel between the two different reactions, the orientation of the product molecules in channel 1 of the H^++HD reaction is more apparent than in its isotopic reaction D^++HD. However, in channel 2, the orientations of the product molecules are similar for the two reaction systems. This indicates that either intramolecular or the intermolecular isotopic substitution can affect the product polarizations of the reaction systems.

Figure 6 shows the angular momentum polarization in the form of polar plots $p(\theta_r,\phi_r)$, which represents the full average distribution of $P(\omega_t, \omega_r)$ of the scattering angle. We can see that the distribution of $p(\phi_r,\phi_r)$ mainly peaks at (π/2, π/2) and (π/2, 3π/2), and this is in good agreement with the distributions of $P(\theta_r)$ and $P(\phi_r)$. These distributions of p (θ_r,ϕ_r) indicate that the H_2, HD, and D_2 products are preferentially polarized perpendicular to the scattering plane, and these reactions are dominated by "in-plane" mechanisms.

Finally, we note that the overall product alignment shown in the present work is rather weak. This is especially apparent in Fig. 4, where the alignment at intermediate collision angles is rather low, and in Fig. 3c–d, where the calculated values are close to zero. Very interestingly, in a previous quantum study by Zanchet et al. [45], a similar finding was reported for the H^++D_2 reaction. Their quantum study showed that the calculated alignment values of the product HD are nearly always close to zero at almost all scattering angles for the H^++ $D_2(v,j)\rightarrow HD(v',j')$ + D^+ reaction at a translational energy of 0.524 eV, thus clearly indicating that **j′** and **k′** are randomly aligned. Thus, our present stereodynamics study based on QCT calculations has further corroborated this argument from the previous quantum study.

Conclusions

The quasi-classical trajectory method has been employed to investigate the isotopic effects on the reactions H^++HD and D^++HD using the ground KBNN PES at a collision energy of 0.7 eV. The polarization-dependent differential cross-section and the distributions of $p(\theta_r)$ and $p(\phi_r)$ have been calculated. Comparison of the total reaction probability with J=0 for the H^++D_2 reaction shows good agreement with the wavepacket exact quantum-mechanical result. The distributions of $P(\phi_r)$ right-handed product rotation in planes parallel to the scattering plane for these reactions. It was also found that the mass factor plays an important role in product rotation, with different effects on product's rotational alignment for different reaction types. For the D^++HD reaction, the mass factor increases from channel 2 to channel 1, and the distribution of the product's rotational angular momentum becomes less anisotropic, while increasing the mass factor enhances the anisotropy of the distribution of **j′** for the H^++HD reaction. For channel 1 in both reactions, H^++HD and D^++HD, the isotropic distribution of **j′** increased with increasing mass factor, but in channel 2 the isotropic distribution of **j′** decreased with increasing mass factor. Aside from the mass factor, other factors, such as the lifetime of the complex and the threshold energy, can also influence the polarizations of the products for these reactions.

References

1. Miller S, Tennyson J (1992) Chem Soc Rev 21:281–288
2. Jambrina PG, Aoiz FJ, Bulut N, Smith SC, Balint-Kurti GG, Hankel M (2010) Phys Chem Chem Phys 12:1102–1115
3. Ochs G, Teloy E (1974) J Chem Phys 61:4930–4931
4. Gerlich D, Nowotny U, Schlier C, Teloy E (1980) Chem Phys 47:245–255
5. Schlier C, Nowotny U, Teloy E (1987) Chem Phys 111:401–408
6. Ichihara A, Yokoyama K (1995) J Chem Phys 103:2109–2112
7. Takayanagi T, Kurosaki Y, Ichihara A (2000) J Chem Phys 112:2615–2622
8. Kamisaka H, Bian W, Nobusada K, Nakamura H (2002) J Chem Phys 116:654–665
9. Chu TS, Han KL (2005) J Phys Chem A 109:2050–2056
10. Lu RF, Chu TS, Han KL (2005) J Phys Chem A 109:6683–6688
11. Viegas LP, Alijah A, Varandas AJC (2007) J Chem Phys 126 (074309):1–9
12. Amaran S, Kumar S (2008) J Chem Phys 128(064301):1–11
13. Wrede E, Schnieder L, Seekamp-Schnieder K, Niederjohann B, Welge KH (2005) Phys Chem Chem Phys 7:1577–1582
14. Song H, Dai DX, Wu GR, Wang CC, Harich SA, Hayes MY et al (2005) J Chem Phys 123(074314):1–10
15. Chu TS, Han KL (2008) Phys Chem Chem Phys 10:2431–2441
16. Chu TS, António AJC, Han KL (2009) Chem Phys Lett 471:222–228
17. Gonzalez-Lezana T, Aguado A, Paniagua M, Roncero O (2005) J Chem Phys 123(194309):1–13
18. Gonzalez-Lezana T, Roncero O, Honvault P, Launay JM, Bulut N, Aoiz FJ et al (2006) J Chem Phys 125(094314):1–13
19. Li B, Chu TS, Han KL (2010) J Comput Chem 31:362–370
20. Song H, Wang XY, Skodje RT, Yang XM (2006) Chin J Chem Phys 19:375–378
21. Li B, Han KL (2008) J Chem Phys 128(114116):1–7
22. Geballe TR, Tennyson J, Oka T (2006) Philos Trans R Soc London Ser A 364:2847-2853
23. Herbst E, Oka T, Watson JKG (2000) Philos Trans R Soc London Ser A 358:2363-2369
24. de Miranda MP, Aoiz FJ, Bañares L, Rábanos VS (1999) J Phys Chem 111:5368–5383
25. Hsu DSY, Weinstein ND, Herschbach DR (1975) Mol Phys 29:57–278
26. Aoiz FJ, Martínez MT, Rábanos VS (2001) J Phys Chem 114:8880–8896
27. de Miranda MP, Clary DC, Castillo JF, Manolopoulos DE (1998) J Chem Phys 108:3142–3153
28. de Miranda MP, Pogrebnya SK, Clary DC (1999) Faraday Discuss 113:119–132
29. Mcclelland GM, Saenger KL, Valentini JJ, Herschbach DR (1979) J Phys Chem 83:947–959

30. Barnwell JD, Loeser JG, Herschbach DR (1983) J Phys Chem 87:2781–2786
31. Truhlar DG, Muckerman JT (1979) Atom–molecule collision theory. Plenum, New York
32. Han KL, He GZ, Lou NQ (1996) J Chem Phys 105:8699–8704
33. Shafer-Ray NE, Orr-Ewing AJ, Zare RN (1995) J Phys Chem A 99:7591–7603
34. Li XH, Wang MS, Pino I, Yang CL, Ma LZ (2009) Phys Chem Chem Phys 11:10438–10445
35. Wang ML, Han KL, He GZ (1998) J Phys Chem A 102:10204–10210
36. Wang ML, Han KL, He GZ (1998) J Chem Phys 109:5446–5454
37. Brouard M, Lambert HM, Rayner SP, Simons JP (1996) Mol Phys 89:403–423
38. Chu TS, Zhang Y, Han KL (2006) Int Rev Phys Chem 25:201–235
39. Han KL, He GZ (2007) J Photochem Photobiol C 8:55–66
40. Han KL, He GZ, Lou NQ (1993) Chin Chem Lett 4:517–520
41. Wang ML, Han KL, Zhan JP, Wu VWK, He GZ, Lou NQ (1997) Chem Phys Lett 278:307–312
42. Chen MD, Han KL, Lou NQ (2002) Chem Phys Lett 357:483–490
43. Li RJ, Han KL, Li FE, Lu RC, He GZ, Lou NQ (1994) Chem Phys Lett 220:281–285
44. Han KL, Zhang L, Xu DL, He GZ, Lou NQ (2001) J Phys Chem A 105:2956–2960
45. Zanchet A, Roncero O, Gonzàlez-Lezana T, Rodríguez-López A, Aguado A, Sanz-Sanz C, Gómez-Carrasco S (2009) J Phys Chem A 113:14488–14501